



OPEN

SUBJECT AREAS:

APPLIED PHYSICS
ELECTRONIC DEVICESReceived
17 April 2014Accepted
19 August 2014Published
10 September 2014Correspondence and
requests for materials
should be addressed to
H.W.L. (hwliang@dlut.
edu.cn)* These authors
contributed equally to
this work.

Low Al-composition p-GaN/Mg-doped $\text{Al}_{0.25}\text{Ga}_{0.75}\text{N}/n^+$ -GaN polarization-induced backward tunneling junction grown by metal-organic chemical vapor deposition on sapphire substrate

Kexiong Zhang^{1*}, Hongwei Liang^{1*}, Yang Liu¹, Rensheng Shen¹, Wenping Guo², Dongsheng Wang¹, Xiaochuan Xia¹, Pengcheng Tao¹, Chao Yang¹, Yingmin Luo¹ & Guotong Du^{1,3}¹School of Physics and Optoelectronic Engineering, Dalian University of Technology, Dalian 116024, China, ²Jiangsu Xinguanglian Technology Co., Ltd., Wuxi 214192, China, ³State Key Laboratory on Integrated Optoelectronics, School of Electronic Science and Engineering, Jilin University, Changchun 130012, China.

Low Al-composition p-GaN/Mg-doped $\text{Al}_{0.25}\text{Ga}_{0.75}\text{N}/n^+$ -GaN polarization-induced backward tunneling junction (PIBTJ) was grown by metal-organic chemical vapor deposition on sapphire substrate. A self-consistent solution of Poisson-Schrödinger equations combined with polarization-induced theory was used to model PIBTJ structure, energy band diagrams and free carrier concentrations distribution. The PIBTJ displays reliable and reproducible backward tunneling with a current density of 3 A/cm^2 at the reverse bias of -1 V . The absence of negative differential resistance behavior of PIBTJ at forward bias can mainly be attributed to the hole compensation centers, including C, H and O impurities, accumulated at the p-GaN/Mg-doped AlGaN heterointerface.

Inter-band tunneling junction (TJ) is a type of interesting vertical quantum transport device, which presents a negative differential resistance (NDR) behavior under forward bias and an ohmic characteristic rather than a rectification characteristic under reverse bias¹. NDR behavior in TJ enables a variety of attractive applications in low-power memory, logic circuit, high-speed switching and high-frequency oscillation up to terahertz range²⁻⁴. Backward diode, a modification of TJ, presents an excellent frequency response and can be used in microwaves detection, small signals rectification and frequency mixing⁵⁻⁷. In addition, TJ is a critical component in electrically connecting multiple active regions of devices such as multi-color light emitting diodes (LEDs), laser diodes (LDs), photo-detectors and tandem solar cells (SCs)^{8,9}.

Owing to their high thermal stability, high breakdown voltage, high radiation hardness and high electron saturation velocity, III-V nitrides have great potential in fabricating vertical quantum transport devices, including the inter-band TJ¹⁰. However, efficient inter-band TJ is still a challenging issue for wide-band-gap GaN and AlGaN materials, mostly due to the large width and height of tunneling barrier. Moreover, the Mg dopant solubility limits, low acceptor ionization efficiency and severe self-compensation effect of Mg-doped III-V nitrides at room temperature (RT) makes it hard for the realization of degenerate hole concentration¹¹. Recently, the investigations of AlGaN/GaN high electron mobility transistors (HEMTs) have demonstrated that two-dimensional electron gas (2DEG) with degenerate concentration can be induced at the AlGaN/GaN heterointerface, due to the effect of polarization charges^{12,13}. Furthermore, during the theoretical study of metal-AlGaN/GaN heterostructure, Singh *et al.* predicted that the large band bending and degenerate 2DEG induced by the polarization charges at the undoped AlGaN/GaN heterointerface makes possible a new type of TJ with tailored tunneling probabilities and current-voltage (I-V) characteristics^{14,15}. Theoretically, for a GaN/AlGaN/GaN heterostructure, a two-dimensional hole gas (2DHG) also can be induced at the upper GaN/AlGaN heterointerface

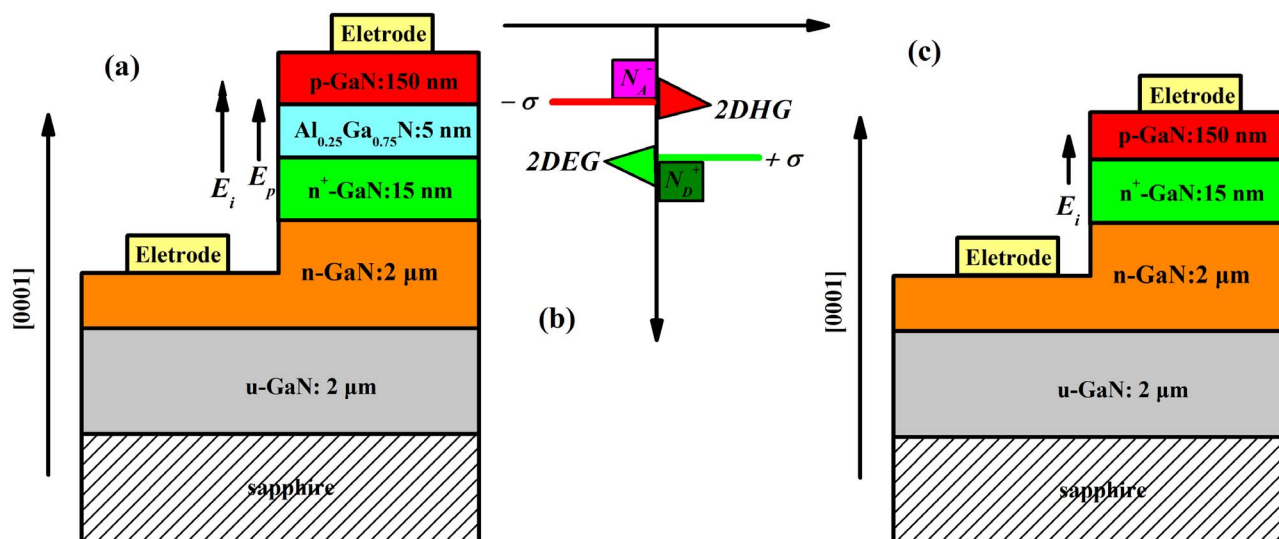


Figure 1 | (a) Schematic diagram of sample A and (b) spatial distributions of fixed polarization charges, ionized dopants and free mobile carriers gas in sample A and (c) schematic diagram of sample B.

with the similar carrier concentration as that of 2DEG at the lower AlGaN/GaN heterointerface¹⁶. The simultaneous appearance of degenerate polarization-induced 2DEG and 2DHG in GaN/AlGaN/GaN heterostructure can enable interband tunneling process. Based on this concept of polarization-induced theory, III-V nitrides inter-band polarization-induced TJ (PITJ) in the form of forward NDR device and backward diode has been successfully verified experimentally and theoretically by some research groups using Al-polar AlN or N-polar In-rich InGaN as a polarization-induced layer^{17–22}. Simon *et al.* introduced a Al-polar GaN/AlN/GaN PITJ, demonstrating backward diode characteristic with reverse current density of 750 mA/cm² at 0.8 V¹⁹. Alternatively, Krishnamoorthy *et al.* achieved PITJ with forward NDR effect and backward tunneling characteristics using high In-composition N-polar InGaN^{20–22}. These results are very encouraging for the design and fabrication of III-V nitrides TJ with eliminating the need of degenerate p-type doping, which is a general requirement for traditional TJ and also a significant problem for wide-band-gap III-V nitrides. However, due to the high barrier height, the wide band gap of AlN in GaN/AlN/GaN PITJ reduces tunneling probability greatly, resulting in low current density and high tunneling resistance^{19,20}. While narrow band gap InGaN in GaN/InGaN/GaN PITJ leads to additional tunneling band discontinuities at the GaN/InGaN heterojunction, which is expected to reduce the overall tunneling probability^{21,22}. In addition, the optical absorption loss of InGaN layer impedes the application of InGaN-based PITJ into optoelectronics device like tandem SCs and UV emitters^{21,22}. Furthermore, the above mentioned PITJs were all grown on GaN templates by molecular beam epitaxy (MBE) using Al-polar AlN or N-polar In-rich InGaN. Though most commercial III-V nitrides optoelectronic devices are grown on sapphire substrates by metal-organic chemical vapor deposition (MOCVD) nowadays, the growth of III-V nitrides PITJ by MOCVD using Al-polar AlN and N-polar In-rich InGaN is not an easy task due to the difficult control of surface morphology, crystalline quality and impurities incorporation of materials²³. In view of the tradeoffs of Al-polar AlN-based and N-polar In-rich InGaN-based PITJ, it may be expected that Ga-polar AlGaN with low Al-composition, owing lower tunneling barrier height and better optical transparency, is an ideal candidate for the efficient inter-band tunneling in III-V nitrides material, since the growth and doping of Ga-polar AlGaN with low Al-composition (<30%) on sapphire substrates by MOCVD are easy and commercially available with smooth surface morphology and excellent crystalline quality^{24,25}. Especially, in our recent report, using Ga-polar low

Al-composition Mg-doped Al_{0.15}Ga_{0.85}N as a polarization-induced layer, an obvious NDR behavior with high peak-to-valley current ratio of about 9 and peak current of 22.4 mA (~current density of 11.4 A/cm²) at 3.67 V was realized in p-GaN/Mg-doped Al_{0.15}Ga_{0.85}N/n⁺-GaN heterostructure grown by MOCVD on sapphire substrate²⁶. Though the backward tunneling current density was found to be low, it still reveals the possibility of growing Ga-polar AlGaN-based PITJ with low Al-composition on sapphire substrate by MOCVD.

In this study, using Mg-doped Al_{0.25}Ga_{0.75}N interlayer combined with n⁺-GaN, a low Al-composition p-GaN/Mg-doped Al_{0.25}Ga_{0.75}N/n⁺-GaN PITJ was grown by MOCVD on planar sapphire substrate using conventional GaN epitaxial processing. The physical mechanism of p-GaN/Mg-doped Al_{0.25}Ga_{0.75}N/n⁺-GaN PITJ was presented through calculations based on self-consistent solution of Poisson-Schrödinger equations combined with polarization-induced theory. Repeatable and efficient inter-band tunneling was achieved with a current density of 3 A/cm² at the reverse bias of -1 V. The influence of hole compensation centers accumulated at the p-GaN/Mg-doped Al_{0.25}Ga_{0.75}N interface on the forward current-voltage (I-V) characteristic of PITJ was also discussed.

Results

During their investigation of Al_{0.28}Ga_{0.72}N/GaN heterostructure, Singh *et al.* revealed that there was a compromise between the thickness of polarization-induced layer and the tunneling probability^{14,15}. The density of states (DOS) in polarization-induced charges at the heterointerface increases with the increase of the thickness of AlGaN. However, the tunneling probability through the barrier is low for a thick polarization-induced layer according to the Wentzel-Kramers-Brillouin (WKB) model²⁷. Thus, considering the low Al-composition of AlGaN used in our study, the thicknesses of AlGaN was fixed at 5 nm which is thick enough to allow high DOS in polarization-induced charges and thin enough to allow high tunneling probability. Fig. 1(a) and Fig. 1(c) is the schematic diagram of the p-GaN/Mg-doped Al_{0.25}Ga_{0.75}N/n⁺-GaN PITJ, named sample A and the reference sample, a p-GaN/n⁺-GaN junction, named sample B. To investigate the physical mechanism of PITJ, simulations of sample A and sample B were performed using self-consistent solution of Poisson-Schrödinger equations combined with the polarization-induced theory. The material parameters adopted during the simulations can be found in the Ref. 28.



According to polarization-induced theory of III-V nitrides, a thin strained Mg-doped $\text{Al}_{0.25}\text{Ga}_{0.75}\text{N}$ interlayer surrounded by a GaN p-n⁺ junction in sample A will induce a polarization dipole layer with high densities of fixed polarization charges $\pm\sigma$ ($\sim 10^{13}/\text{cm}^2$) at the upper GaN/AlGa_{0.25}N and lower AlGa_{0.25}N/GaN heterointerface, respectively²⁹. As shown in the Fig. 1(b), these high densities of fixed polarization charges combined with ionized dopants constitute the total space charges in the depletion region of sample A. To balance these ionized dopants and the fixed polarization charges, 2DHG and 2DEG are accumulated with degenerate concentration at the upper GaN/AlGa_{0.25}N and lower AlGa_{0.25}N/GaN heterointerface, respectively. The calculated equilibrium band diagram of sample A shown in the Fig. 2(a) verifies that there exists potential-wells for electrons at the upper GaN/AlGa_{0.25}N and holes at the lower AlGa_{0.25}N/GaN heterointerface, respectively. The inset of Fig. 2(a) shows that the potential-well depths for 2DEG and 2DHG are 263 and 127 meV, respectively. Furthermore, as shown in Fig. 2(b), the concentrations of 2DEG and 2DHG are 5.85×10^{19} and $6.6 \times 10^{19} \text{ cm}^{-3}$, respectively, which meet the requirements of degenerate carrier concentrations of III-V nitrides Tj³⁰. In contrast, the concentrations of electrons and holes of sample B shown in the Fig. 3(b) are less than 10^{18} and 10^{19} cm^{-3} , respectively, which is far lower than those of sample A. Moreover, the polarization electric field E_p created by the polarization dipole in sample A can assist the built-in electric field E_i (in the same direction of E_p) created by ionized dopants dipole, which introduces a total electric field as high as $\sim 10^6 \text{ V/cm}^{19}$. This strong total electric field lead to extremely large band bending and would enable the alignment of energy bands over a very narrow depletion region across the GaN p-n junction. The inset in Fig. 2(a) proves that the giant electric field shrinks the depletion region width to a thickness less than 8 nm closing to the thickness of AlGa_{0.25}N interlayer, which is lower than the depletion region width of sample B, presenting a thickness of 20 nm as shown in the inset of Fig. 3(a). Therefore, it can be found that the carrier concentrations and depletion region width of sample B are far from satisfactory for tunneling process, due to the lack of polarization-induced effect of AlGa_{0.25}N interlayer.

Because of the strong quantum-confinement effect of two potential wells in sample A, 2DEG and 2DHG are distributed in the confined potential-well states. At the thermal equilibrium state, there is an overlap of energy levels between the conduction band on the n-side and the valence band on the p-side. If the electrons energy levels of 2DEG in the potential well coincide with one of the holes energy levels of 2DHG, carriers can tunnel between conduction band and valence band, leading to the formation of tunneling current³¹. When a forward-bias voltage is applied to the sample A, the concentrations

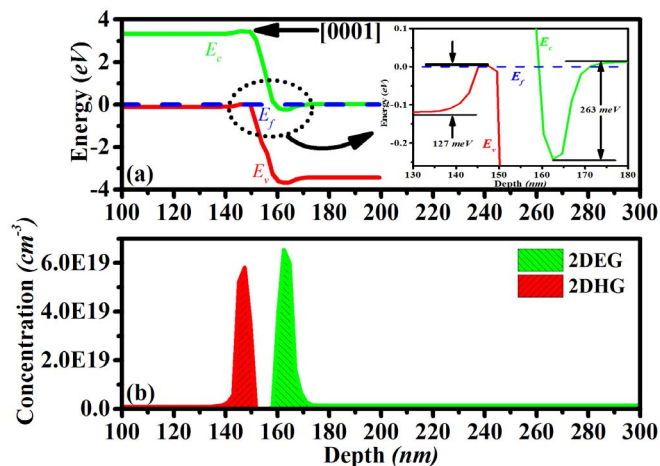


Figure 2 | (a) Energy band diagrams and (b) carrier distributions of sample A at equilibrium state. The inset shows the detail view of band diagram at the tunneling region.

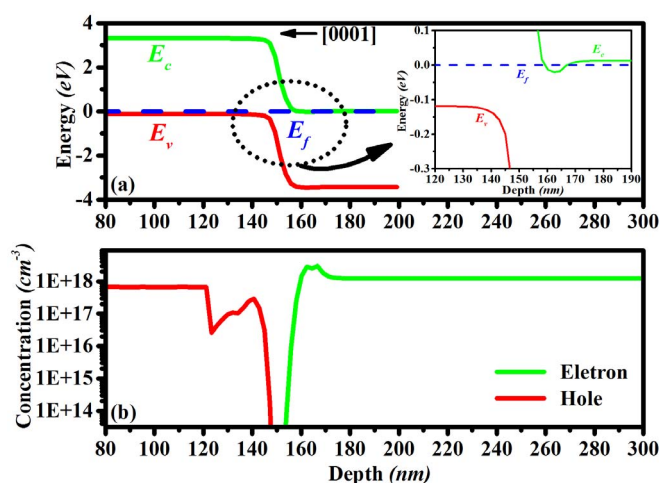


Figure 3 | (a) Energy band diagrams and (b) carrier distributions of sample B at equilibrium state. The inset shows detail view of band diagram at the space charge region.

of degenerate carrier gases increase and electrons inject from the n-side to the p-side, causing the increase of tunneling current. With further increasing forward bias to 0.3 V (as shown in the Fig. 4(a)), the Fermi level E_f under thermal equilibrium conditions splits into two different quasi-Fermi levels E_f^n and E_f^p for electrons and holes, respectively. Conduction and valence bands are no longer aligned and NDR effect is expected to happen. The concentrations of 2DEG and 2DHG at 0.3 V shown in the Fig. 4(b) are 5.9×10^{19} and $6.7 \times 10^{19} \text{ cm}^{-3}$, respectively. Moreover, the inset in Fig. 4(a) shows that the potential-well depths of 2DEG and 2DHG at 0.3 V are 272 and 133 meV, respectively. The deeper potential-wells at forward bias are attributed to the increasing accumulation of 2DEG and 2DHG. At a higher forward bias, tunneling current ceases and diffusion current becomes the dominant. On the other hand, when a reverse-bias voltage of -0.3 V is applied to the sample A, the conduction band edge on the n-side is pulled below the valence band edge on the p-side, as shown in the Fig. 5(a). Valence band electrons from occupied states on the p-side can tunnel into the unoccupied states in the conduction band of n-side, leading to the great increase of reverse tunneling current. Though high densities of valence band electrons keep tunneling from p-side to n-side, electrons and holes are quickly swept out of the potential wells due to the driven effect of reverse-bias

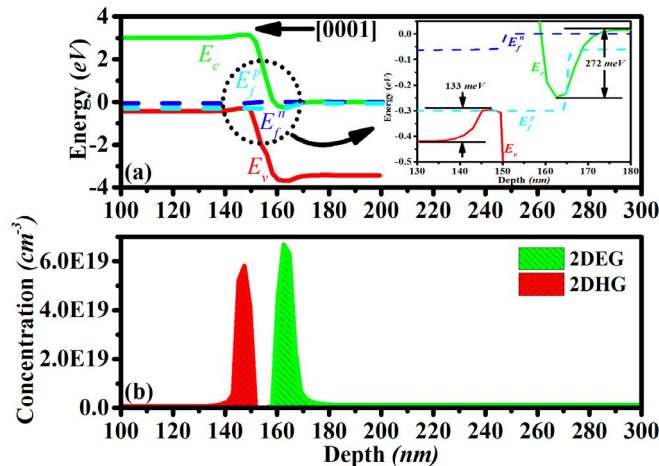


Figure 4 | (a) Energy band diagrams and (b) carrier distributions of sample A at +0.3 V. The inset shows the detail view of band diagram at the tunneling region.

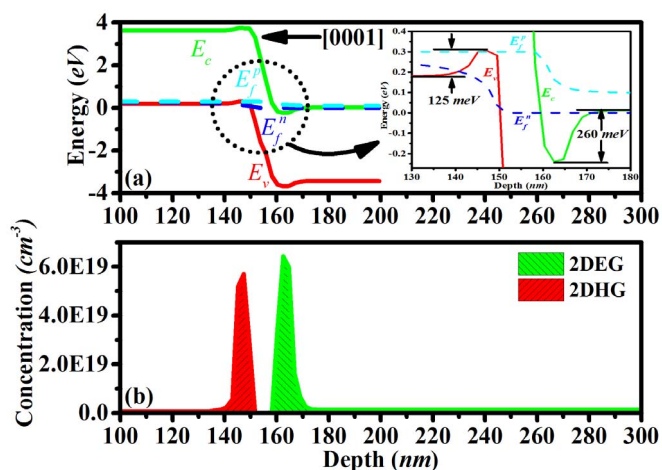


Figure 5 | (a) Energy band diagrams and (b) carrier distributions of sample A at -0.3 V. The inset shows the detail view of band diagram at the tunneling region.

electric field. Therefore, as shown in the Fig. 5(b), the concentrations of 2DEG and 2DHG at -0.3 V are 5.7×10^{19} and $6.4 \times 10^{19} \text{ cm}^{-3}$, respectively, which are a little lower than those at thermal equilibrium state. In addition, the inset in Fig. 5(a) shows that the potential-well depths of 2DEG and 2DHG at -0.3 V are 260 and 125 meV, respectively.

Fig. 6 presents the ω - 2θ XRD scans of the Mg-doped $\text{Al}_{0.25}\text{Ga}_{0.75}\text{N}/\text{GaN}$ SLs. The distinct satellite peaks up to second order indicate that the SLs are in good crystalline quality and abrupt interface. According to the formula from Ref. 32, the Al-composition and thickness of AlGa_n interlayer are calculated to be 25% and 5 nm, respectively, indicating a good agreement with the simulation conditions during the self-consistent solution of Schrödinger and Poisson equations. The root-mean-square (RMS) roughness of sample A, as shown in the inset of Fig. 6 is 0.42 nm over a scan area of $2 \times 2 \mu\text{m}^2$ with an obvious atomically flat terraces-and-steps structure, demonstrating a smooth surface morphology.

Discussion

Fig. 7 shows RT I–V curves of sample A and sample B taken by consecutively forward sweeping from -4 up to 4 V while measuring the current through the device. The positive bias is defined when applying a positive voltage on the p-GaN layer. For the I–V curve shown in the inset of Fig. 7, the sample B presents a usual diode

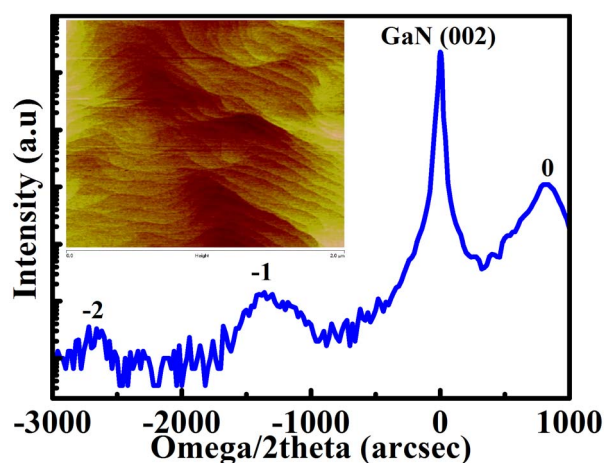


Figure 6 | The ω - 2θ XRD scans of p-AlGaIn/GaN SLs. The left inset shows the surface morphology of sample A.

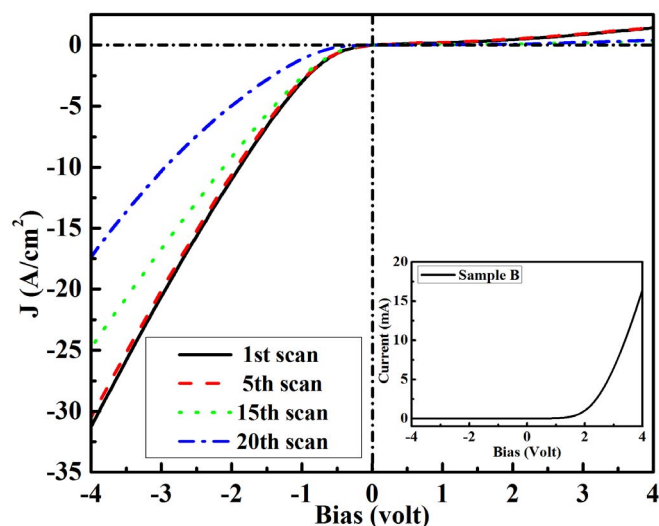


Figure 7 | The I–V curves of sample A under consecutive scans. The right inset shows the I–V curves of sample B.

rectifying behavior with a very low reverse current. On the other hand, the I–V curves of sample A show much higher reverse current than that in the forward direction with a strong nonlinearity at zero bias, which is a typical behavior of a backward diode. Backward diode is a type of TJ in which the forward current (including the NDR region) is suppressed greatly compared with reverse current³³. Therefore, the I–V characteristics comparison between two samples demonstrate that tunneling process is actually generated by inserting $\text{Al}_{0.25}\text{Ga}_{0.75}\text{N}$ strain layer into p-GaN/ n^+ -GaN junction. We have to point out that, just like the phenomenon in metal-semiconductor Schottky contact, as a heterostructure with multiple dielectric layers for sample A, there is a possibility that the image effect of 2DEG may also impose some influence on the tunneling process^{34–36}. However, according to the study of A Minj *et al.*, image force and image charges only play a major role when the size or electrode contact area of device is at the nanoscale, such as in the size of a few square nanometers³⁵. Considering the device size of sample A ($\sim 200 \times 150 \mu\text{m}^2$), the effect of image charges can be neglected in this study. Moreover, as pointed out by A. A. Grinberg, the image force induced by 2DEG is quite different from that in metal-semiconductor contact based on the following two points³⁶. Firstly, the image force lowering of the heterointerface barrier by 2DEG is smaller than it would be in a metal-semiconductor contact. Secondly, the influence of image force induced by 2DEG on the interface barrier remains finite even though their distance from the surface or interface goes to zero. Therefore, tunneling process can't be realized only through image force or image potential, since the image charges alone are not enough to decrease the tunneling height and width in our work. From the above discussions, it can be concluded that the polarization-induced effect of AlGa_n interlayer plays a dominant role in the tunneling process and the generation of 2DHG and 2DEG, which also excludes the possibility of Schottky tunneling between the electrode and p-GaN.

As shown in the Fig. 7, the reliability and reproducibility of PITJ were studied via twenty scans of I–V characteristics with no significant degradation of the device performance, in contrast to our previous report of NDR device²⁶. The enhanced reproducibility with consecutive scans can be attributed to the improved crystalline quality of PITJ, especially the AlGa_n interlayer, which decreases stress relaxation and thereby dislocations densities. Though slight degradation of reverse tunneling current are still happened after twenty scans, a more stable I–V characteristic can be obtained through the further optimization of layers structure and material growth conditions. However, the I–V characteristics of sample A just present



backward diode behavior without NDR phenomenon at forward bias, which seems to contradict with the theory of PITJ and our above simulation results. Generally, tunneling current of TJ with generate carrier concentrations in forward and backward directions increases, as the electric field increases and depletion width decreases. The backward tunneling current only involves normally filled valence band electrons from the p-side tunneling into normally empty conduction states on the n-side. However, the forward tunneling current depends on the carrier concentrations for providing available conduction electrons in the n-side and available empty states in the p-side⁷. Hence, it can be concluded that the p-side of sample A is not quite degenerate as the n-side, resulting in the decrease of available empty states in the p-side, which may be associated with the increase of hole compensation centers. Generally speaking, the decrease of carrier concentrations is mainly due to the compensation effect of defects, including dislocations and impurities. As reported by Simon and Krishnamoorthy, similar I–V characteristics without negative differential resistance (NDR) phenomenon at forward bias have also been observed in the PITJ with Al-polar GaN/AlN/GaN and N-polar GaN/InGaN/GaN structures grown on GaN templates by MBE^{19,20}. In view of the lower dislocation densities and better interface quality of their samples than those of our sample A grown on planar sapphire substrate by MOCVD, the still absence of NDR phenomenon in their samples indicates that dislocations and interface states don't play a dominant role in the compensation of hole concentration. Moreover, since the thickness of AlGaIn interlayer in sample A was less than the critical thickness, the influence of strain relaxation and the related dislocations and interface states can be neglected in this study. Therefore, the reason for the similarity of I–V characteristic between our work and Simon and Krishnamoorthy's samples may lie in the distribution of impurities, since AlN and N-polar III–V nitrides are easily susceptible to the incorporation of impurities.

To verify our reasoning, SIMS was taken to analyze the distribution of impurities in sample A. In our study, the minimum size of SIMS sputtering-spot was about $100 \times 100 \mu\text{m}^2$, which was at the same level of device size as that of sample A. The impurities distributions at a sputtering point can actually provide the average information of spatial distributions of impurities in a sputtering plane. Therefore, the SIMS data can be used to analyze the influence of the planar distributions of impurities on the sheet charges. As shown in Fig. 8, in the SIMS study of p-GaN/Mg-doped $\text{Al}_{0.25}\text{Ga}_{0.75}\text{N}$ heterointerface, an accumulation of C, H and O impurities happens near the p-GaN/Mg-doped $\text{Al}_{0.25}\text{Ga}_{0.75}\text{N}$ heterointerface. The C, H and O concentrations at the heterointerface are 6×10^{18} , 1.5×10^{19} and $5 \times 10^{17} \text{cm}^{-3}$, respectively. The high levels of H can be explained by the formation of Mg–H complexes, since H incorporation is in tandem with Mg doping³⁷. The incorporation of O originates largely from NH_3 , easily forming strong chemical bond with Al³⁸. The possible source of C impurities are from the decomposition of metal-organic precursors, CO and CO_2 contaminants in the NH_3 , and hydrocarbons resulting from H_2 etching of SiC coated graphite susceptors³⁹. Moreover, the accumulation of C, H and O impurities at the heterointerface can be attributed to the growth interruption after the growth of Mg-doped $\text{Al}_{0.25}\text{Ga}_{0.75}\text{N}$ to adjust growth condition for p-GaN^{40–41}. During the growth interruption, the residual Mg and Al in the reactor are accumulated on the surface of Mg-doped $\text{Al}_{0.25}\text{Ga}_{0.75}\text{N}$, which will promote the adsorption of impurities^{40–42}. In addition, as can be seen in the SIMS data, the C, H, O impurities show the similar variation trend as the change of depth, which illustrates the spatial diffusion or distribution traces of impurities. Impurities may diffuse along the dislocations and vacancies and gather at the heterointerface, which also increase the impurities incorporation in the heterointerface⁴³. Though SIMS data alone can't tell us whether the impurities are interstitial or substitutional, the most favorable sites for impurities in material depend on their formation energies as a function of growth stoichiometry and

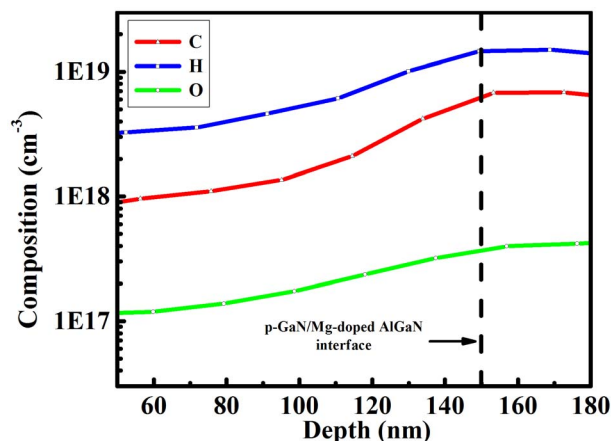


Figure 8 | SIMS depth profiles in sample A for C, H and O atomic concentrations at p-GaN/Mg-doped $\text{Al}_{0.25}\text{Ga}_{0.75}\text{N}$ heterostructure interface.

Fermi level, which can be calculated by first-principles theory or, to be specific, density-functional theory (DFT)^{39,44}. Firstly, C_{Ga} (C substituted at a Ga site) is found to be a shallow donor while C_{I} (C at an interstitial site) exhibits deep donor behavior in p-type GaN³⁹. Using DFT, A. F. Wright presented that the formation energies of C_{Ga} and C_{I} are lower than that of substitutional C_{N} (C substituted at a N site) in Mg-doped p-type GaN, making it likely that both C_{Ga} and C_{I} are preferred sites in p-GaN³⁹. However, C_{I} is favored under Ga-rich growth conditions while C_{Ga} is preferred under N-rich growth conditions^{39,44}. In light of the N-rich conditions during the growth of p-GaN and AlGaIn by MOCVD, C_{Ga} would be more preferred^{39,44}. Secondly, DFT calculations indicate that Mg–H complex and isolated H^+ should be the dominant H species in p-type Mg-doped GaN⁴⁵. Mg–H complex was known to play a crucial role in passivating the Mg acceptors. The calculations by Jörg Neugebauer *et al.* present that H acts as a donor (H^+) in p-type GaN, and as an acceptor (H^-) in n-type material⁴⁶. Thirdly, in a DFT study of O impurities in GaN, A. F. Wright indicated that the formation energies of O_{Ga} (O substituted at a Ga site) and O_{I} (O at an interstitial site) were higher than that of O_{N} (O substituted at a N site) for all values of the Fermi level, suggesting that O_{N} , being a single donor, is the dominant and most stable O state in p-type GaN⁴⁷. Moreover, O_{N} can either compensate a Mg_{Ga} acceptor or combine with it to form $(\text{Mg}_{\text{Ga}}\text{O}_{\text{N}})^0$ complex. Therefore, the above discussions indicate that C, H and O impurities in the p-GaN and AlGaIn behave dominantly as donor in the form of C_{Ga} , Mg–H complex or H^+ , and O_{N} , respectively.

The enhanced incorporation of C, H and O impurities, behaving as donors in p-type material, will increase the background concentrations of electrons and hole compensation in the p-side. As a result, a high degree of hole compensation is expected to be happened in the region around 2DHG, which reduces the degenerate degree of 2DHG. Therefore, when a reverse bias is applied, electrons could easily tunnel from the valence band of the p-side into the conduction band of the n-side, which leads to the increase of a tunneling current in the backward direction. However, under forward bias, as the band overlapping is not significant considering the different degree of degeneration of 2DEG and 2DHG, the tunneling vanishes in the forward direction and NDR effect will not appear. Forward diffusion current across the p–n junction becomes the dominant process with depressed tunneling current. Due to the relatively high barrier height of $\text{Al}_{0.25}\text{Ga}_{0.75}\text{N}$ for carrier transition, the forward current of sample A is lower than that of sample B at the same bias value, which also leads to the increase of turn-on voltage of sample A. Though the impurities compensation can be considered as the dominant compensation mechanism, the influence of other impurities, such as N



vacancies, are not discussed in the study. Therefore, more detailed investigations are needed to further explore the hole compensation centers and their effect on the performance of PITJ, which are beneficial for the freely modulating the generate degree of 2DHG at the p-side to conveniently fabricate different device characteristics of GaN-based PITJ for forward NDR behavior or backward tunneling property.

The PITJ studied here exhibits current density in the 3–30 A/cm² range at the reverse bias between −1 V and −4 V, which is low for III-nitrides optical emitters such as LEDs and LDs. To further increase the tunneling current, decreasing heterointerface hole compensation centers, adjusting the thickness of polarization dipole layer and optimizing material epitaxial processing are needed. Moreover, the performance improvement by hybrid using low Al-composition AlGa_{0.25}N and low In-composition InGa_{0.75}N layers (to grow structures like n-GaN/p-AlGa_{0.25}N/p-InGa_{0.75}N and n-InGa_{0.75}N/p-AlGa_{0.25}N/p-InGa_{0.75}N) can also greatly increase the polarization charges profiles and thus the tunneling current.

Conclusions

In summary, the design of PITJ using low Al-composition AlGa_{0.25}N interlayer combined with n⁺-GaN was confirmed by theoretical simulations and experimental results. The PITJ displays reliable and reproducible backward tunneling with a current density of 3 A/cm² at the reverse bias of −1 V. The absence of NDR behavior of PITJ at the forward bias can be attributed to the hole compensation centers, such as C, H and O impurities, accumulated at the p-GaN/Mg-doped AlGa_{0.25}N heterointerface. The PITJ demonstrated in this work can balance optical transparency and tunneling probability simultaneously, which is also compatible with the currently commercial III-V nitrides epitaxial processing. Low Al-composition AlGa_{0.25}N-based PITJ opens up new opportunities for the performance improvement of III-V nitrides optoelectronics devices in multi-color LEDs, LDs, and tandem SCs, and also holds much promise for future applications in GaN-based microwave detectors, inter-band vertical transport quantum devices, and terahertz oscillators.

Methods

Samples fabrication. For the experimental studies, sample A and sample B were grown on planar c-plane sapphire substrates using conventional GaN epitaxial method by MOCVD with an Aixtron close coupled showerhead system. Trimethylgallium (TMGa), trimethylaluminum (TMAI), and ammonia (NH₃) were used as Ga, Al, and N precursors, respectively. Biscyclopentadienyl magnesium (Cp₂Mg) and silane (SiH₄) were used as p-type and n-type GaN dopants, respectively. The structure of sample A consists of a 2 μm undoped GaN, 2 μm GaN:Si (Si ~ 4 × 10¹⁸ cm⁻³), 15 nm GaN:Si (Si ~ 4 × 10¹⁹ cm⁻³), 5 nm Al_{0.25}Ga_{0.75}N:Mg (Mg ~ 5.5 × 10¹⁹ cm⁻³), 150 nm GaN:Mg (Mg ~ 6 × 10¹⁹ cm⁻³). The sample B has the similar structure as sample A but without Al_{0.25}Ga_{0.75}N interlayer. After growth, the samples were annealed in the O₂ ambient at 750 °C for 15 min. Diodes with a size of 200 × 150 μm² were fabricated on the whole 2-inch wafers. Ni/Au (20/150 nm) and Ti/Al/Ni/Au (20/100/40/50 nm) stacks were evaporated using standard optical lithography on the p-GaN and n-GaN layers, respectively.

Measurements. Al-composition and epilayer thickness determination of sample A were investigated and calibrated using high resolution X-ray diffraction (HRXRD from Bede D1) by growing 20 period Mg-doped Al_{0.25}Ga_{0.75}N/GaN (5 nm/7 nm) SLs at the same growth condition, thickness and Al-composition as sample A. The surface morphology of sample A was viewed by atomic force microscope (AFM from Veeco D3100) with a tapping mode. I-V electrical properties of two samples were characterized at RT with I-V analyzer (Keithley Model 2611A). A secondary ion mass spectroscopy (SIMS from CAMECA IMS-7f) was used to probe the concentrations of element in the samples.

1. Esaki, L. New phenomenon in narrow germanium p-n junctions. *Phys. Rev.* **109**, 603–604 (1958).
2. Chung, S.-Y. *et al.* Three-terminal Si-based negative differential resistance circuit element with adjustable peak-to-valley current ratios using a monolithic vertical integration. *Appl. Phys. Lett.* **84**, 2688–2690 (2004).
3. Alibart, F. & Strukov, D. B. Utilizing NDR effect to reduce switching threshold variations in memristive devices. *Appl. Phys. A* **111**, 199–202 (2013).

4. Wernersson, L.-E., Årlelid, M., Egard, M. & Lind, E. Gated tunnel diode in oscillator applications with high frequency tuning. *Solid-State Electron.* **53**, 292–296 (2009).
5. Takahashi, T., Sato, M., Hirose, T. & Hara, N. Energy band control of GaAsSb-based backward diodes to improve sensitivity of millimeter-wave detection. *Jpn. J. Appl. Phys.* **49**, 104101 (2010).
6. Xie, Y. W., Sun, J. R., Guo, D. F., Shen, B. G. & Zhang, X. Y. Backward diode behavior in oxygen-excessive manganite-titanate p-n junction. *Europhys. Lett.* **87**, 57006 (2009).
7. Schulman, J. N., Chow, D. H. & Jang, D. M. InGaAs zero bias backward diodes for millimeter wave direct detection. *IEEE Electron Device Lett.* **22**, 200–202 (2001).
8. Lumb, M. P. *et al.* Double quantum-well tunnel junctions with high peak tunnel currents and low absorption for InP multi-junction solar cells. *Appl. Phys. Lett.* **100**, 213907 (2012).
9. Ozden, I., Makarona, E., Nurmikko, A. V., Takeuchi, T. & Krames, M. A dual-wavelength indium gallium nitride quantum well light emitting diode. *Appl. Phys. Lett.* **79**, 2532–2534 (2001).
10. Li, D. *et al.* Repeatable low-temperature negative-differential resistance from Al_{0.18}Ga_{0.82}N/GaN resonant tunneling diodes. *Appl. Phys. Lett.* **100**, 252105 (2012).
11. Monemar, B. *et al.* Evidence for two Mg related acceptors in GaN. *Phys. Rev. Lett.* **102**, 235501 (2009).
12. Wang, L., Kim, D. H., Tanaka & Adesida, I. Direct contact mechanism of Ohmic metallization to AlGa_{0.25}N/GaN heterostructures via Ohmic area recess etching. *Appl. Phys. Lett.* **95**, 172107 (2009).
13. Murphy, M. J. *et al.* High-frequency AlGa_{0.25}N/GaN polarization-induced high electron mobility transistors grown by plasma-assisted molecular-beam epitaxy. *Appl. Phys. Lett.* **75**, 3653–3655 (1999).
14. Singh, M., Zhang, Y., Singh, J. & Mishra, U. Examination of tunnel junctions in the AlGa_{0.25}N/GaN system: consequences of polarization charge. *Appl. Phys. Lett.* **77**, 1867–1869 (2000).
15. Singh, M., Singh, J. & Mishra, U. Current-voltage characteristics of polar heterostructure junctions. *J. Appl. Phys.* **91**, 2989–2993 (2002).
16. AlMustafa, N. *et al.* The coexistence of two-dimensional electron and hole gases in GaN-based heterostructures. *J. Appl. Phys.* **111**, 044512 (2012).
17. Grundmann, M. J. & Mishra, U. K. Multi-color light emitting diode using polarization-induced tunnel junctions. *Phys. Stat. Sol. (c)* **4**, 2830–2833 (2007).
18. Schubert, M. F. Interband tunnel junctions for wurtzite III-nitride semiconductors based on heterointerface polarization charges. *Phys. Rev. B* **81**, 035303 (2010).
19. Simon, J. *et al.* Polarization-induced Zener tunnel junctions in wide-band-gap heterostructures. *Phys. Rev. Lett.* **103**, 026801 (2009).
20. Krishnamoorthy, S. *et al.* Polarization-engineered GaN/InGa_{0.25}N/GaN tunnel diodes. *Appl. Phys. Lett.* **97**, 203502 (2010).
21. Krishnamoorthy, S., Park, P. S. & Rajan, S. Demonstration of forward inter-band tunneling in GaN by polarization engineering. *Appl. Phys. Lett.* **99**, 233504 (2011).
22. Krishnamoorthy, S., Akyol, F., Park, P. S. & Rajan, S. Low resistance GaN/InGa_{0.25}N/GaN tunnel junctions. *Appl. Phys. Lett.* **102**, 113503 (2013).
23. Zhang, L. *et al.* Three-dimensional hole gas induced by polarization in (0001)-oriented metal-face III-nitride structure. *Appl. Phys. Lett.* **97**, 062103 (2010).
24. Huang, G. S., Yao, H. H., Lu, T. C., Kuo, H. C. & Wang, S. C. Aluminum incorporation into AlGa_{0.25}N grown by low-pressure metal organic vapor phase epitaxy. *J. Appl. Phys.* **99**, 104901 (2006).
25. Jeon, S.-R. Investigation of Mg doping in high-Al content p-type Al_xGa_{1-x}N (0.3 < x < 0.5). *Appl. Phys. Lett.* **86**, 082107 (2005).
26. Zhang, K. X. *et al.* Negative differential resistance in low Al-composition p-GaN/Mg-doped Al_{0.15}Ga_{0.85}N/n⁺-GaN hetero-junction grown by metal-organic chemical vapor deposition on sapphire substrate. *Appl. Phys. Lett.* **104**, 053507 (2014).
27. Sze, S. M. *Physics of Semiconductor Devices* (Wiley, New York, 1981).
28. Piprek, J. *Nitride Semiconductor Devices: Principles and Simulation* (Wiley, Darmstadt, 2007).
29. Yasuda, T. *et al.* Investigations of polarization-induced hole accumulations and vertical hole conduction in GaN/AlGa_{0.25}N heterostructures. *Jpn. J. Appl. Phys.* **52**, 08JJ05 (2013).
30. Khokhlev, O. V., Bulashevich, K. A. & Karpov, S. Y. Polarization doping for III-nitride optoelectronics. *Phys. Status Solidi A* **210**, 1369–1376 (2013).
31. Sweeny, M. & Xu, J. M. Resonant interband tunnel diodes. *Appl. Phys. Lett.* **54**, 546–548 (1989).
32. Vashaei, Z., Bayram, C. & Razeghi, M. Demonstration of negative differential resistance in GaN/AlN resonant tunneling diodes at room temperature. *J. Appl. Phys.* **107**, 083505 (2010).
33. Sun, Q. Q. *et al.* The physics and backward diode behavior of heavily doped single layer MoS₂ based p-n junctions. *Appl. Phys. Lett.* **102**, 093104 (2013).
34. Xu, Z. L. Electrostatic interaction in the presence of dielectric interfaces and polarization-induced like-charge attraction. *Phys. Rev. E* **87**, 013307 (2013).
35. Minj, A., Cavalcoli, D. & Cavallini, A. Thermionic emission from the 2DEG assisted by image-charge-induced barrier lowering in AlInN/AlN/GaN heterostructures. *Nanotechnology* **23**, 115701 (2012).
36. Grinberg, A. A. Image potential of a two-dimensional electron gas. *Phys. Rev. B* **32**, 8187–8190 (1985).



37. Kuwano, Y. *et al.* Lateral hydrogen diffusion at p-GaN Layers in nitride-based light emitting diodes with tunnel junctions. *Jpn. J. Appl. Phys.* **52**, 08JK12 (2013).
38. Jang, H. W., Baik, J. M., Lee, M.-K., Shin, H.-J. & Lee, J.-L. Incorporation of Oxygen Donors in AlGaIn. *J. Electrochem. Soc.* **151**, G536–G540 (2004).
39. Wright, A. F. Substitutional and interstitial carbon in wurtzite GaN. *J. Appl. Phys.* **92**, 2575–2585 (2002).
40. Sugita, K., Sasamoto, K., Hashimoto, A. & Yamamoto, A. Effects of Cp_2Mg supply on MOVPE growth behavior of InN. *Phys. Stat. Sol. (c)* **8**, 2506–2508 (2011).
41. Wang, G. T. & Creighton, J. R. Complex formation between Magnesiumocene (MgCp_2) and NH_3 : implications for p-Type doping of group III nitrides and the Mg memory effect. *J. Phys. Chem. A* **108**, 4873–4877 (2004).
42. Koblmüller, G., Chu, R. M., Raman, A., Mishra, U. K. & Speck, J. S. High-temperature molecular beam epitaxial growth of AlGaIn/GaN on GaN templates with reduced interface impurity levels. *J. Appl. Phys.* **107**, 043527 (2010).
43. Tápajna, M., Mishra, U. K. & Kuball, M. Importance of impurity diffusion for early stage degradation in AlGaIn/GaN high electron mobility transistors upon electrical stress. *Appl. Phys. Lett.* **97**, 023503 (2010).
44. Seager, C. H., Wright, A. F., Yu, J. & Götz, W. Role of carbon in GaN. *J. Appl. Phys.* **92**, 6553–6560 (2002).
45. Wright, A. F., Seager, C. H., Myers, S. M., Koleske, D. D. & Allerman, A. A. Hydrogen configurations, formation energies, and migration barriers in GaN. *J. Appl. Phys.* **94**, 2311–2318 (2003).
46. Neugebauer, J. & Van de Walle, C. G. Hydrogen in GaN: novel aspects of a common impurity. *Phys. Rev. Lett.* **75**, 4452–4455 (1995).
47. Wright, A. F. Substitutional and interstitial oxygen in wurtzite GaN. *J. Appl. Phys.* **98**, 103531 (2005).

Acknowledgments

This work was supported by National Natural Science Foundation of China (Nos.61223005,61376046), National High Technology Research and Development Program (863 program) (No.2011AA03A102), the fundamental research funds for the Central Universities (Nos.DUT12LK22,DUT13RC205), the research fund for the doctoral program of higher education (No. 20110041120045).

Author contributions

K.X.Z. carried out the experiments design, the samples growth, theoretical simulations and data analysis. W.P.G. carried out the samples' XRD and AFM measurements. K.X.Z. wrote the manuscript with suggestions from H.W.L. K.X.Z. and H.W.L. revised the manuscript. Y.L., R.S.S., W.P.G., D.S.W., X.C.X., P.C.T., C.Y., Y.M.L. and G.T.D. gave scientific advices. All the authors contributed through scientific discussion and reviewed the manuscript.

Additional information

Competing financial interests: The authors declare no competing financial interests.

How to cite this article: Zhang, K. *et al.* Low Al-composition p-GaN/Mg-doped $\text{Al}_{0.25}\text{Ga}_{0.75}\text{N}/\text{n}^+$ -GaN polarization-induced backward tunneling junction grown by metal-organic chemical vapor deposition on sapphire substrate. *Sci. Rep.* **4**, 6322; DOI:10.1038/srep06322 (2014).



This work is licensed under a Creative Commons Attribution-NonCommercial-NoDerivs 4.0 International License. The images or other third party material in this article are included in the article's Creative Commons license, unless indicated otherwise in the credit line; if the material is not included under the Creative Commons license, users will need to obtain permission from the license holder in order to reproduce the material. To view a copy of this license, visit <http://creativecommons.org/licenses/by-nc-nd/4.0/>